Journal of Computational and Applied Mechanics, Vol. 5., No. 2., (2004), pp. 383–400

EFFECTS OF SWEEP AND SPANWISE CHANGING CIRCULATION APPLIED TO AIRFOILS: A CASE STUDY

János Vad
Department of Fluid Mechanics, Budapest University of Technology and Economics
H-1111 Budapest, Hungary
vad@simba.ara.bme.hu

[Received: February 11, 2004]

Abstract. Isolated stationary airfoils of simple geometry were tested in incompressible flow in order to study the combined aerodynamic effects of sweep, spanwise changing circulation, and their combination. Endwall effects were excluded from the studies. The tool of study was computational fluid dynamics, supplemented with wind tunnel experiments involving laser Doppler anemometry and flow visualisation. The computational results suggested unloading effects due to leading and trailing edge sweep. A model has been proposed for the description of such effects. It has been rendered probable that harmonization of the sweep with the spanwise circulation gradient results in reduction of the fluid pathline length on the suction side, giving a potential for reduction of profile losses.

Keywords: airfoil, axial flow turbomachinery, computational fluid dynamics, controlled vortex design, spanwise changing circulation, sweep

Nomenclature

b	$[m]$	projection of airfoil at midspan
c	$[-]$	force coefficient
c_p	$[-]$	static pressure coefficient
f	$[m]$	camber height
F	$[N]$	force
ℓ	$[m]$	blade chord
LR	$[-]$	lift coefficient ratio
p	$[Pa]$	static pressure
p_t	$[Pa]$	total pressure
s	$[m]$	span
v	$[m/s]$	velocity
y	$[m]$	transverse coordinate
α	$[\circ]$	geometric angle of incidence
λ	$[\circ]$	sweep angle of the stacking line
λ_{EQ}	$[\circ]$	equivalent sweep (equation 5.3)
λ_{LE}	$[\circ]$	leading edge sweep
λ_{TE}	$[\circ]$	trailing edge sweep
ρ	$[kg/m^3]$	air density

ξ	$[-]$	total pressure loss coefficient (equation 5.5)
Γ	$[m^2/s]$	circulation[1]

Subscripts and superscript

$inlet$	at the inlet of the test section
L, D	lift, drag
mid	at 50 percent span (midspan)
PS, SS	pressure side, suction side
SW, USW	swept, unswept
ref	reference
x, y, s	orthogonal coordinates[2]
$\hat{}$	chordwise averaged

1. **Introduction**

An axial flow turbomachinery blade is swept when each blade section of a datum blade with a radial stacking line is displaced parallel to its chord line in a prescribed manner. Backward or forward sweep occurs if a blade section at a given radius is downstream or upstream of the adjacent blade section at lower radius, respectively.

Blade sweep, often combined with dihedral, offers a potential for improvement of turbomachinery stage performance and efficiency, increase of pressure peak, shift of stall margin towards lower flow rate [1], [2], reduction of shock losses [3]; and noise reduction [4]. No general concept exists for prescribing the optimum spanwise blade sweep distribution for best stage efficiency. Only a qualitative guideline – regarding the direction of optimum sweep – can be given, and even the applicability of this guideline is restricted to the near-endwall region. The loss-reducing effects of 'positive sweep' (for which the blade section under consideration is upstream of the adjacent inboard section) are widely acknowledged for the near-endwall blade sections in low-speed rectilinear cascades [5]-[7], in transonic propfan rotors [8], in stators of low-speed compressors [9] and in transonic compressors [10]. This suggests the trend that a high-efficiency blading should have backward sweep near the hub and forward sweep near the tip, as appears in [8], [11], [12].

However, even such a qualitative guideline has not yet been found in the literature regarding optimum sweep for sections further away from the endwalls, as concluded in the CMFF'03 workshop organized in this topic [13]. For parts of blades of large aspect ratio where the flow is less affected by the endwalls, optimization of sweep could be an important issue in efficiency improvement. With the lack of a general concept yielding optimum sweep (design output), designs consider spanwise sweep distribution as input (arbitrarily prescribed) data. Optimum sweep is sought even

[1] integral of velocity on a closed curve surrounding an airfoil section and fitting to a plane normal to the spanwise direction

[2] axial (along the wind tunnel axis), transverse, spanwise (Figure 3)

in the most recent research programs on a trial-and-error basis, by means of testing bladings of various sweep or skew prescribed in an arbitrary manner.

The lack of a general sweep optimization concept manifests itself in apparently contradictory results in the technical literature. Disregarding the advantages of backward sweep near the hub, the studies by most researchers suggest the benefits of forward sweep along the entire span. Such benefits are: higher energy transfer, lower wake losses and better blade element flow [1], better fit to design flow conditions along the entire span [2], reduced shock/boundary layer interaction [3], and generally improved fan performance [4], [11]. In contrast to the concept of leading edge (LE) sweep benefit near the endwalls, it has been reported in [14] that a forward-swept rotor with unswept LE is favorable for obtaining good hydraulic efficiency. There are a few reports opposing the view that forward sweep is advantageous in general. In [8], it has been pointed out that sweep results in a longer path of the fluid particles over the suction surface near midspan, thus increasing the thickness of the suction side boundary layer compared to the case of no sweep. This suggests that, although sweep diminishes shock losses, both forward and backward sweep may result in increased profile losses and reduced efficiency. Studies in [15] and [16] show that both backward and forward sweep reduce the total pressure rise and efficiency, however, the swept-back blading had more regular wake along the entire span and demonstrated better overall characteristics than the forward-swept one.

It is a generally widespread view in the turbomachinery community that the sweep angle and blade circulation distribution along the span are independent design variables. However, a correlation appears to exist between the aerodynamic optimum sweep and the spanwise circulation gradient. Favorable tendencies due to forward sweep have been reported usually in the case of rotors for which a positive spanwise blade circulation gradient was present. This was either due to the controlled vortex design (i.e. total pressure rise increasing along the dominant part of span) [2], [3], [11], [17]; or due to a flow rate lower than design [1], [4]. Unswept blades were proven to be most beneficial for rotors of free vortex operation (negligible spanwise circulation gradient by design) [8], [16]. Measurements in [15], [18] showed that both performance and efficiency were reduced for a swept-forward bladed rotor compared to a swept-back blading. In this case, a slight negative spanwise circulation gradient was present in the swept-forward bladed rotor, due to the only approximate realization of the free vortex design concept.

Similar tendency can be observed in the case of glider or bird wings. Figure 1 shows a lifelike example of presumable aerodynamic optimum combination of sweep and spanwise circulation gradient. The seagull wing has evolved over millions of years to realize a high lift-to-drag ratio, making effective gliding possible. In this paper, the classic sign convention and interpretation in [19] applies, i.e. the sweep angle λ (the angle between the stacking line and the spanwise direction) is positive for backward sweep and is negative for forward sweep. Starting from the body of the bird (nearly zero circulation) up to midspan, increasing circulation dominates ($d\Gamma/ds > 0$). Accordingly, the wing is swept forward ($\lambda < 0$) in this region. Above

midspan, the circulation must decrease along the span ($d\Gamma/ds < 0$) to zero (wing tip). During evolution, backward sweep ($\lambda > 0$) has been developed for this wing section.

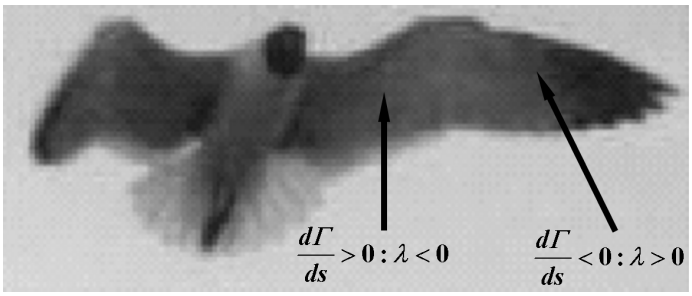

Figure 1. Seagull wing

As a step towards a concept for aerodynamic optimum harmonization of sweep and spanwise changing circulation in turbomachine design, this paper presents a case study for exploration of fluid mechanical effects due to sweep, spanwise changing circulation, and their combination applied to airfoils, with exclusion of endwall and compressibility effects. The case study has been carried out by means of Computational Fluid Dynamics (CFD) supplemented by wind tunnel experiments involving laser Doppler anemometry (LDA) and flow visualization. Preliminary studies have been reported in [20]. Isolated stationary airfoils of simple geometry are studied herein and similar qualitative behavior is assumed for rotating cascade arrangements, as in [5]. The former studies presented in the literature on swept airfoils and cascades usually aimed at the investigation of endwall effects. Furthermore, the loading [19] or camber geometry [6], [7] was constant with span, i.e. no attention was paid to the combined effects of sweep and spanwise changing circulation farther from the endwalls.

2. **Test airfoils**

The subjects of the present investigation are four airfoils, either unswept (US) or backward-swept (BS), and either of spanwise nearly constant circulation (CC) or spanwise decreasing circulation (DC) at midspan. The airfoils have been labelled accordingly, as shown in Figure 2. In Figure 2, the vertical upward direction is considered to be spanwise direction. During the experiments, each airfoil was placed in a single airfoil configuration in a wind tunnel section of rectangular cross-section $430\,mm \times 520\,mm$ in such a way that the airfoil root and tip extended to the tunnel walls ($s = 430\,mm$) and the airfoil was located in the tunnel mid-plane. The coordinate system is indicated in Figure 3a.

Each airfoil consists of geometrically similar circular arc plate sections parallel to the xy plane. The data of such airfoil sections are presented in Table 1. The leading and trailing edges (LE, TE) have been rounded. US/CC was used as a reference. The

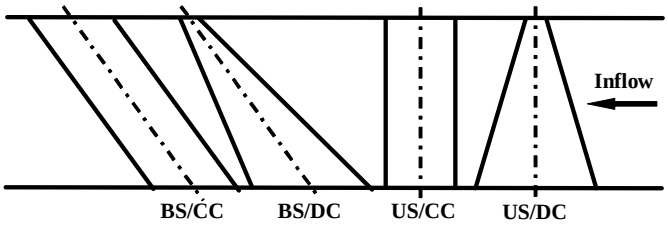

Figure 2. Scheme of airfoils

camber geometry and the geometrical angle of incidence (angle between the far-field upstream velocity and the chord) result in a lift coefficient of 0.740 and a maximum lift-to-drag ratio of approximately 40 for US/CC in two-dimensional (2D) tests [21]. BS/CC and BS/DC are swept backward, i.e. the consecutive blade sections along the span have been shifted toward the relative downstream direction, parallel to their chord. The capabilities of the wind tunnel limited the mean axial velocity set in the test to $10.0\,m/s$, and this value was used as reference velocity v_{ref}. The chord decreases linearly along the span in the cases of US/DC and BS/DC. The Reynolds number calculated with midspan chord, reference velocity, and kinematical viscosity of air at $20\,^{\circ}C$ was $1.13 \cdot 10^5$ during the tests. This relatively low value may raise the question of whether laminar separation occurs on the airfoils. The experiments and, consistently, the CFD runs showed no evidence for separation, supported also by the fact that the airfoil sections were adjusted to the angle providing maximum lift-to-drag ratio for the 2D airfoil test case [21]. The Mach number computed with reference velocity and speed of sound in air at $20\,^{\circ}C$ was 0.03 and therefore, the flow was considered truly incompressible. It is not an objective of this paper to report on problems related to compressibility or on shock loss reduction by means of appropriate sweep. The midspan chord length, lift coefficient, and sweep angle of the stacking line (the line passing through the airfoil section centers of gravity) were set to values equal to those valid for the case study in [22].

This paper reports studies on the behavior of the airfoils at 50 percent span only, where the endwall effects were found negligible. As is known, the shed vorticity due to the presence of endwalls induces downwash/upwash and thus effective spanwise changes of bound circulation. Computations on the endwall effects have been carried out for US/CC and BS/CC using the method proposed in [19]. These computations showed that the modification of incidence due to downwash perturbation fell below 1 percent of the geometrical angle of incidence 60 percent chord length farther from the endwalls. Considering the aspect ratio $s/\ell_{mid} = 2.53$, this implies that endwall effects are negligible near midspan in the cases studied. Computed pressure distributions on the suction and pressure surfaces and LDA wake measurements at different spanwise locations also showed that near-endwall fluid mechanical effects, for example due to LE and TE inclined to the spanwise direction [27], practically do not affect the flow field near midspan.

Table 1. Airfoil data

Airfoil	**US/DC**	**US/CC**	**BS/DC**	**BS/CC**
λ	$0°$	$0°$	$35°$	$35°$
$d\ell/ds$	-0.572	0	$-0,572$	0
Common data				
Rel. curvature (camber height-to-chord ratio): $f/\ell = 0.04$				
Camber angle: $18.28°$				
Plate thickness: $2.0\,mm$				
Span: $s = 430.0\,mm$				
Midspan chord: $\ell_{mid} = 170.0\,mm$				
Aspect ratio: $s/\ell_{mid} = 2.53$				
Geometrical angle of incidence: $\alpha = 3.3°$				
Lift coefficient (2D airfoil): $c_L = 0.740$				
Axial inlet velocity (reference velocity): $v_{ref} = 10.0\,m/s$				

The force coefficient for either lift or drag force acting on an elementary airfoil section parallel to the xy plane and having spanwise height ds is defined as follows:

$$c_{L,D} = \frac{dF_{L,D}}{ds\ \ell\ (\rho/2)\, v_{ref}^2}, \tag{2.1}$$

where L and D represent lift and drag, respectively.

The circulation around such an airfoil section, in accordance with the Kutta-Joukowski theorem, can be approached as follows:

$$\Gamma = \frac{dF_L}{ds\ \rho\ v_{\mathrm{ref}}} = \frac{c_L\, ds\, \ell\ \rho\ v_{\mathrm{ref}}^2\,/\,2}{ds\ \rho\ v_{\mathrm{ref}}} = \frac{c_L\ \ell\ v_{\mathrm{ref}}}{2}. \tag{2.2}$$

Near midspan, the endwall effects and the downwash/upwash due to trailing shed vorticity were found negligible for US/DC and BS/DC, resulting in a constant incidence (practically equal to the geometrical angle of incidence). This, together with the constant camber relative curvature, yields a spanwise constant lift coefficient in the midspan region. Since the reference velocity is also constant along the span, the spanwise decreasing circulation has been represented by spanwise decreasing chord near midspan for US/DC and BS/DC, quantified by $d\ell/ds$, as indicated in Table 1.

3. **CFD technique**

The wind tunnel tests have been simulated by means of the commercial finite-volume CFD code FLUENT 6 [23]. Figure 3 shows the structured computational mesh for BS/DC as an example, together with an enlarged view of the mesh near the LE. The mesh structure is similar for the TE. The computational domain extends to 3 and 8 ℓ_{mid} upstream and downstream of the airfoil section at midspan, respectively. The total number of nodes is 50 in the spanwise direction. There are 34 nodes in the transverse direction farther from the airfoils, and 30 refined additional nodes have

been applied in the vicinity of the airfoil, both on the suction side (SS) and the pressure side (PS). In the axial direction, 30 nodes are applied upstream of the wing, 8 refined nodes are in the vicinity of both the LE and TE, 20 nodes are along the chord, and 100 nodes are in the downstream section. This amounts to a total number of cells of approximately 800 000, being a compromise with the limited computational infrastructure. When elaborating the grid structure, with special regard to the near-blade region, the guidelines obtained in international collaboration on carefully optimized turbomachinery CFD tools [14], [17], [18], [24] have been followed.

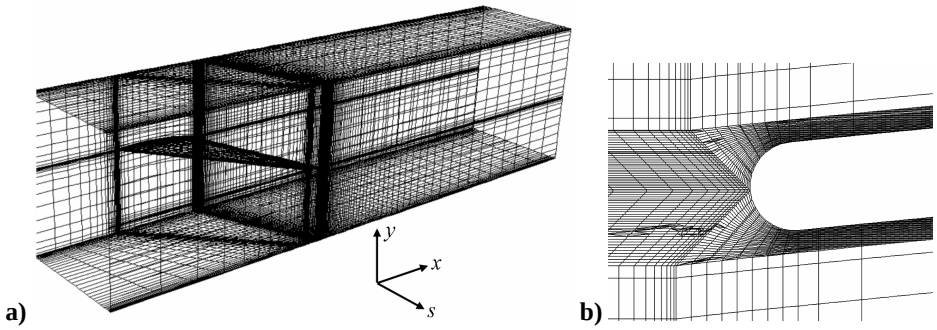

Figure 3. **a)** Computational mesh for airfoil BS/DC, **b)** Enlarged view of near-LE region

The turbulence model elaborated by Spalart and Allmaras [25] has been used because it is acknowledged to give good results for wall-bounded flows and boundary layers subjected to adverse pressure gradients. It has been successfully applied in advanced design systems of swept-bladed turbomachinery [26].

As the LDA measurements revealed, the inlet velocity was practically axial and uniform in the wind tunnel (nearly equal to v_{ref}), and the inlet turbulence intensity was 0.5 percent. These data have been applied as inlet conditions in the CFD studies. A fixed static pressure has been used as the outlet condition.

4. **Experiments**

The wind tunnel experiments were carried out in the National Physics Laboratory (NPL) type wind tunnel at the Department of Fluid Mechanics, Budapest University of Technology and Economics. An inlet contraction with honeycombs and static pressure taps for flow rate measurements, followed by a $1.3\,m$-long straight duct, precedes the test section. The $0.8\,m$-long test section is equipped with glass endwalls for optical access during LDA measurements. The airflow is induced by an axial fan of variable speed $2\,m$ downstream of the test section. An ILA flowPOINT fp50-fus LDA system was connected to the test section. The diameter and the length of the LDA probe volume are 0.3 and $3.3\,mm$, respectively. The flow was seeded with oil

droplets of mean diameter $1.5\,\mu m$ by means of a DANTEC Fog 2005 Loop seeding generator.

LDA measurements were carried out upstream and downstream of the airfoils in order to obtain inlet data for CFD and to check the airfoil wake structure. Five hundred pieces of data were collected for each measuring point. The capability of the CFD technique can be critically evaluated by means of comparison of the CFD and LDA results obtained in the wake. The computed and measured transverse distributions of axial velocity v_x in the wake regions at midspan, 6 percent midspan chord downstream of the TEs, non-dimensionalized by the axial reference velocity v_{ref}, viewed from the downstream direction, are presented in Figure 4. The estimated experimental uncertainty of the LDA measurements is 0.5 percent. The transversal coordinate y has been non-dimensionalized by the b width of projection of the airfoils onto the ys plane at midspan. The velocity profiles are arranged in such a way that the minimum axial velocity appears at $y/b = 0$. The PS and SS wake regions can be seen at $y/b < 0$ and $y/b > 0$, respectively (also for Figure 8). As the Figure shows, the width of the wakes is approximately equal to b, behaving as expected in absence of separation, and the SS wake region is wider, in accordance with the thickened SS boundary layer near the TE. The wake velocity structure is practically identical for each airfoil, within the uncertainty range dedicated to geometrical and alignment uncertainties. The agreement between CFD and LDA data is satisfactory in the middle of the wake. More significant discrepancy can be observed farther away, which could have probably been reduced with repeated attempts on further optimization of the grid. Thus, the computation was considered to be an acceptable basis for only a qualitative comparison of loss behavior.

The flow in the boundary layers of BS/DC has been visualized by emission of a white tracer liquid at midspan near the LE, similarly to the technique applied in [6]. The experimental results, compared to computed pathlines, are shown in Figure 5. The experimental and CFD results are in satisfactory agreement, representing the upward and weak downward flow on the PS and SS, respectively, developing in accordance with the trailing shed vorticity due to spanwise decreasing circulation.

5. **Computational results and discussion**

In the following, the discussion is based on the computed results. Figure 6 shows the computed static pressure distribution on the surface of the airfoils at 50 percent span, represented by the static pressure coefficient

$$c_p = \frac{p - p_{\,\mathrm{ref}}}{(\rho/2)\, v_{\mathrm{ref}}^2}\ , \tag{5.1}$$

where $p_{\,\mathrm{ref}}$ is a reference pressure. Data points of larger absolute value near the LE are not shown.

Considering that $c_L \approx \hat{c}_{p\,PS} - \hat{c}_{p\,SS}$, the lift coefficients were calculated on the basis of the data in Figure 6 and are presented in Table 2. In the case of US/CC, the computed lift coefficient is in satisfactory agreement with the nominal value of

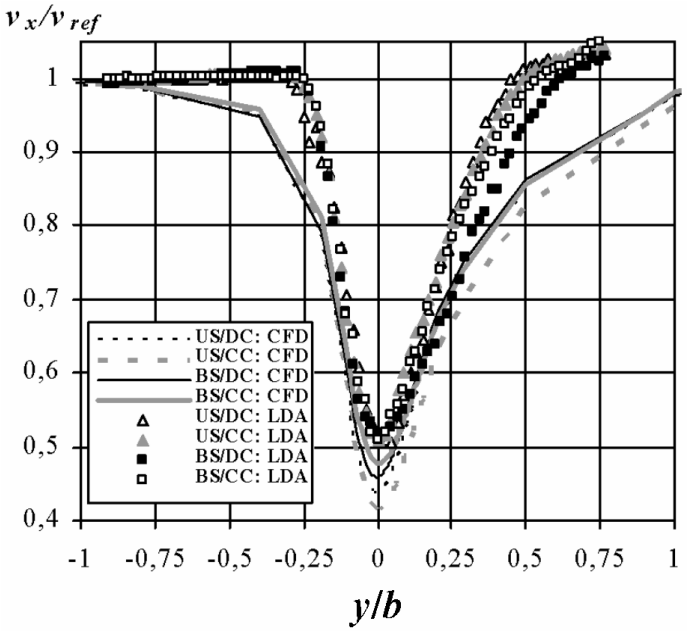

Figure 4. Axial velocity in the wake region

0.740 obtained for the 2D test case (see Table 1). The departure is probably due to the approximations in CFD modelling, as well as numerical integral-averaging of the pressure coefficients along the chord and computation of the lift coefficient from pressure coefficients. The satisfactory agreement confirms the applicability of the CFD tool at the present state of research and also that neglect of endwall effects – also regarding the sidewalls – is reasonable in the region under investigation. Such confirmation can also be made on the basis of the fact that the ratio between the lift coefficients BS/CC and US/CC is 0.81. This value approaches $\cos \lambda = 0.82$ with high accuracy, fitting to the theory stating that, if uncorrected, sweep tends to reduce the lift by the factor of $\cos \lambda$ for airfoils of infinitely large aspect ratio (no endwall effects) [1], [11], [19]. This theory, termed herein 'classic $\cos \lambda$ law', can be easily explained by resolving the incoming flow into components parallel to and perpendicular to the stacking line, parallel to both the LE and TE in the case of BS/CC.

Table 2. Geometrical and computed aerodynamic characteristics

Airfoil	**US/DC**	**US/CC**	**BS/DC**	**BS/CC**
c_L	0.736	0.797	0.657	0.643
λ_{LE}	16.0°	0°	44.6°	35°
λ_{TE}	−16.0°	0°	22.4°	35°
λ_{EQ}	16.0°	0°	33.5°	35°

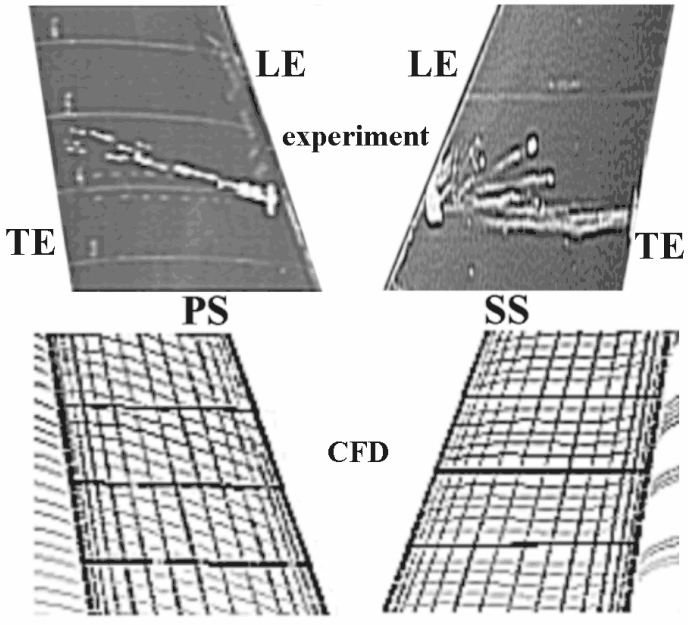

Figure 5. Experimentally and computationally visualized pathlines past airfoil BS/DC

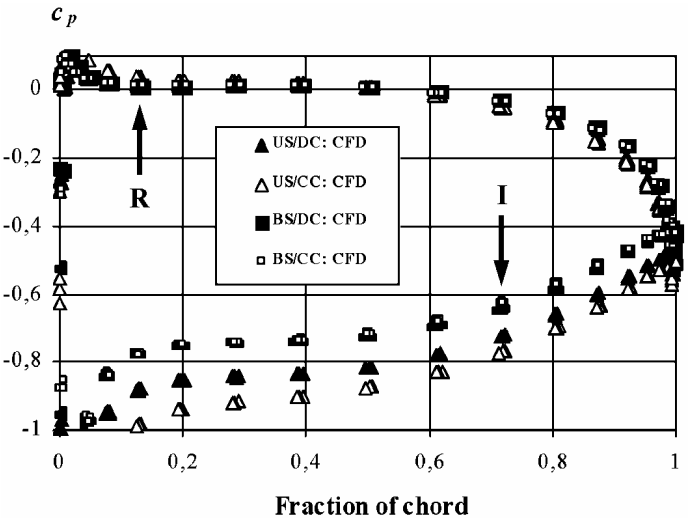

Figure 6. Computed pressure coefficient distribution

It can be observed in Figure 6 and in Table 2 that, although no sweep of stacking line has been applied, US/DC also produces reduced lift compared to US/CC. Furthermore, a slight increase of load can be observed for BS/DC compared to BS/CC on the SS after mid-chord. This effect manifests itself in reduced c_p values on the SS between mid-chord and the TE (indicated by arrow and label 'I' in Figure 6), whereas the pressure is practically equal on the PS. In contrast, the load between the LE and mid-chord of BS/DC is slightly reduced compared to that of BS/CC (slightly reduced pressure on the PS, indicated by arrow and label 'R' in Figure 6; and equal pressures on the SS). The dominance of increased load after mid-chord results in a slightly increased lift for BS/DC vs. BS/CC.

For explanation of these phenomena, the angles between the airfoil edges and the spanwise direction have been calculated and presented in Table 2 as leading edge sweep (λ_{LE}) and trailing edge sweep (λ_{TE}). The sign convention (positive and negative angles for backward and forward sweep, respectively) has consequently been applied.

Based on the above observations, it can be concluded that regardless of the sweep of the stacking line, the sweep of both airfoil edges originating from their inclination to the spanwise direction may cause local unloading of the airfoil. The local unloading can be interpreted similarly to the classic cos λ law: resolving the flow into components parallel to and perpendicular to the LE or TE, only the perpendicular component contributes to the lift. The larger the sweep, the higher the unloading (e.g. LE sweep in sequence for US/CC, US/DC, BS/CC and BS/DC), and reduced sweep causes increased loading (e.g. TE sweep for BS/DC vs. BS/CC). Deliberate use of sweep for unloading the blade LE near the endwalls has been discussed in [27]. However, such effects away from the endwalls have been disregarded, and no TE sweep phenomena have been reported. As the observations presented herein suggest, LE and TE sweep may also be used deliberately farther from the endwalls in order to realize a more favorable load distribution along the chord.

The above suggests that the cos λ law may be extended to airfoil or blade geometries for which both the LE and TE may have sweep, although the stacking line is not necessarily swept.

The lift coefficient ratio LR is introduced as the ratio between lift coefficient $c_{L\,SW}$ of a swept airfoil section (with LE and/or TE sweep) and that of an unswept 2D airfoil $c_{L\,USW}$ (no LE and/or TE sweep, US/CC in the case investigated). Unloading effects of LE and/or TE sweep are expressed in the present case study by means of LR. The following relationships are proposed for LR in order to make a comparison possible with the classic cos λ law:

$$LR = \frac{c_{L\,SW}}{c_{L\,USW}} = \cos\lambda_{EQ}, \tag{5.2}$$

where the equivalent sweep is defined as

$$\lambda_{EQ} = \frac{|\lambda_{LE}| + |\lambda_{TE}|}{2}\,. \tag{5.3}$$

The diagram corresponding to equation (5.2), compared with the LR results computed for the presently investigated airfoils of various λ_{EQ} (summarized in Table 2), is presented in Figure 7a. For comparison, Figure 7b presents the correlation between the computed data and the classic cos λ law stating that

$$LR = \frac{c_{L\,SW}}{c_{L\,USW}} = \cos\lambda\ . \tag{5.4}$$

The sparseness of data points must be acknowledged; the present discussion is to be supported by further tests in the future. Still, the following observations can be made. Both diagrams show the linear trendlines fitted to the data points with use of the least squares method, together with the coefficient of determination R^2. Despite the simple model in equation (5.2), it appears to represent the test results better than the classic cos λ law: in Figure 7a, no inclination and only moderate shift of trendline is observed compared to the plot of equation (5.2); and R^2 is closer to unity. Better agreement could be achieved by: i) considering the streamline inclination modifying the effective angles of sweep; ii) considering that fluid particles along the inclined streamlines pass regions of various local lift in the case of US/DC and BS/DC, due to the spanwise changing geometry.

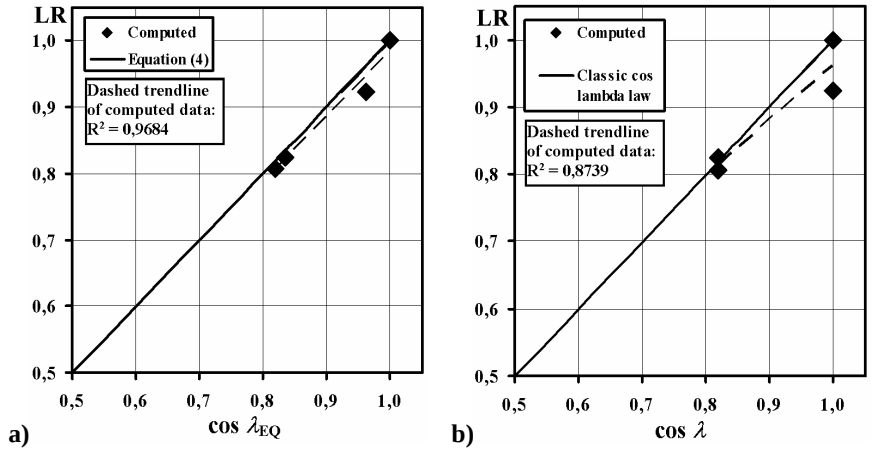

Figure 7. Comparison of **a)** equation (4), **b)** the classic cos λ law with computed data

The ratio between the lift coefficients for BS/DC and US/DC is 0.89. If intending to correct the lift reduction of BS/DC due to sweep using the classic cos λ law (on the basis of stacking line sweep angle $\lambda = 35°$), one would realize that a correction by $\cos\lambda = 0.82$ would overshoot the required lift. Instead, $(\cos\lambda)^{0.58} = 0.89$ would give an appropriate correction. This is in agreement with the results in [11]. Based on several computations, the authors found that fans designed with a sweep correction of $(\cos\lambda)^{0.62}$ instead of cos λ achieved the prescribed pressure rise more accurately.

Beside the effects of finite aspect ratio, the model in equation (5.2) may contribute to the explanation of this observation. Based on [28], it can be established that the rotors studied in [11] had blades with chord decreasing along the span, resulting in LE and TE sweep and thus, in non-zero λ_{EQ} even if the stacking line was unswept ($\lambda = 0$). Therefore, a lift reduction was present even in the reference bladings of unswept stacking line (equation 5.2), and sweep correction moderate compared to $\cos\lambda$ was found sufficient to retain this reduced lift.

Figure 8 shows the distribution of total pressure loss coefficient at midspan, 6 percent midspan chord downstream of the TEs. This characteristic was calculated as follows:

$$\xi = \frac{p_{t\,inlet} - p_t}{(\rho/2)\, v_{ref}^2} \,. \tag{5.5}$$

US/CC appears to generate the highest losses, implying that the drag is the largest for this airfoil. However, it must also be noted that the lift of US/CC is also the largest, probably resulting in reasonably high lift-to-drag ratio. Regarding the airfoil series of US/CC, US/DC and BS/CC, a reduction of total pressure loss can be observed.

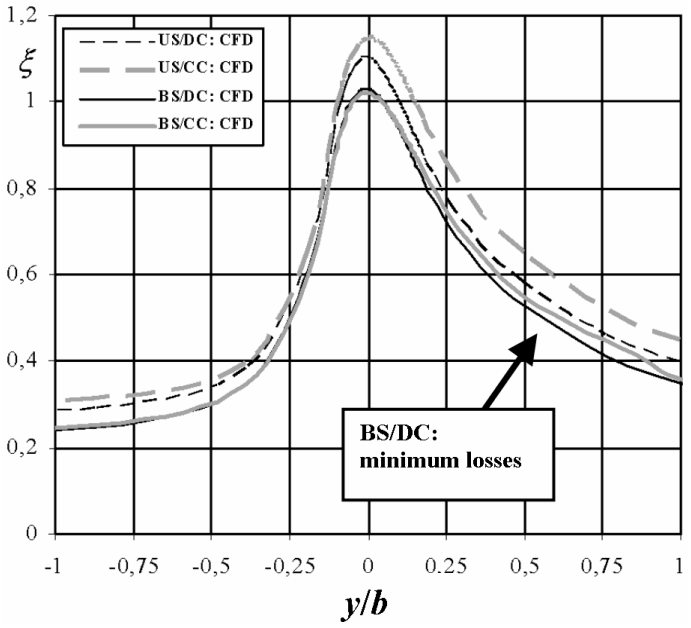

Figure 8. Computed total pressure loss distribution in the wake region

Further reduction of total pressure loss appears on the SS of BS/DC, compared to BS/CC (indicated by an arrow in Figure 8). In the following, causes of this favourable effect are investigated. For qualitative evaluation, Figure 9 presents the

map of computed ξ distributions for BS/CC and BS/DC, including the airfoil part of 75 percent to 100 percent chord. The black regions represent the airfoil. The light grey zones in the SS boundary layer and in the wake correspond to increased losses. The losses are moderate on the SS along the entire represented zone of BS/DC, suggesting that a favourable phenomenon is in effect for this airfoil after mid-chord. As Figure 6 suggests, the chordwise pressure gradient is moderate on the SS from 50 to 80 percent chord for BS/DC compared to BS/CC. This is due to the increased load of BS/DC after mid-chord since its TE is less swept (see Table 2). Such reduction of the adverse pressure gradient appears to reduce the losses. However, one would expect increased losses in the zone of 80 to 100 percent chord where the chordwise pressure gradient is higher in the case of BS/DC. Since Figure 9 shows moderate losses of BS/DC also near the TE, another beneficial effect must be presumed. A possible explanation follows.

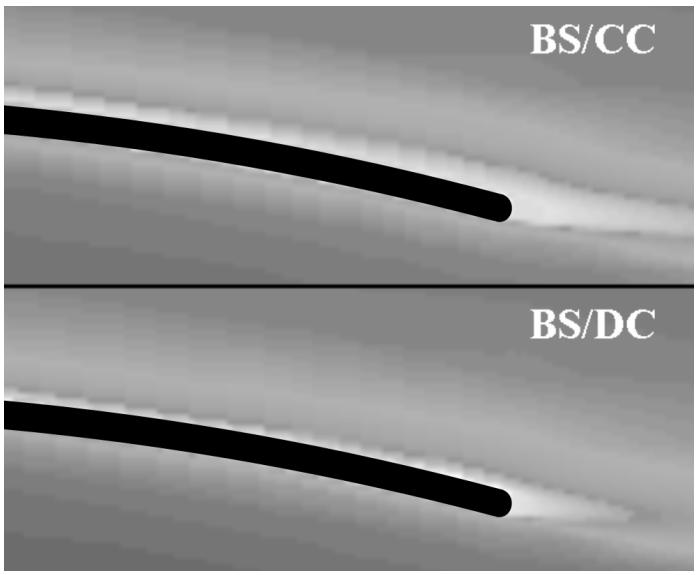

Figure 9. Computed total pressure loss map near the trailing edges

As suggested by the results in [8], the longer path of the fluid particles on the suction surface results in increased losses since the wall friction is more effective along the longer path. Figure 10a shows computed pathlines at the edge of SS boundary layers of BS/CC and BS/DC at midspan, in the region of 75 percent to 100 percent chord. In order to make the inclination of pathlines more visible, the sketches have been compressed to 25 percent in the chordwise direction. The arrows indicate the direction of pathlines at the TE. Due to spanwise constant circulation, no trailing vortices are shed from the TE of BS/CC. This results in SS pathlines parallel to the inflow near the TE of BS/CC. In contrast, trailing shed vorticity is present in the case

of BS/DC due to spanwise decreasing circulation, manifesting itself in SS pathlines inclined downward. (Spanwise increasing circulation would result in upward flow on the SS, as experienced, for example, in [29].) Due to the swept-back TE and downward inclined streamlines for BS/DC, the particles reach the TE along a shorter path. This is a possible explanation of reduced losses also near the TE. Spanwise increasing circulation would elongate the pathlines in the case of a swept-back TE, potentially leading to increased losses. The simplified sketch in Figure 10b illustrates these effects in the vicinity of the TE in a lifelike manner. The case of swept-forward TE could be interpreted in an 'upside down' configuration.

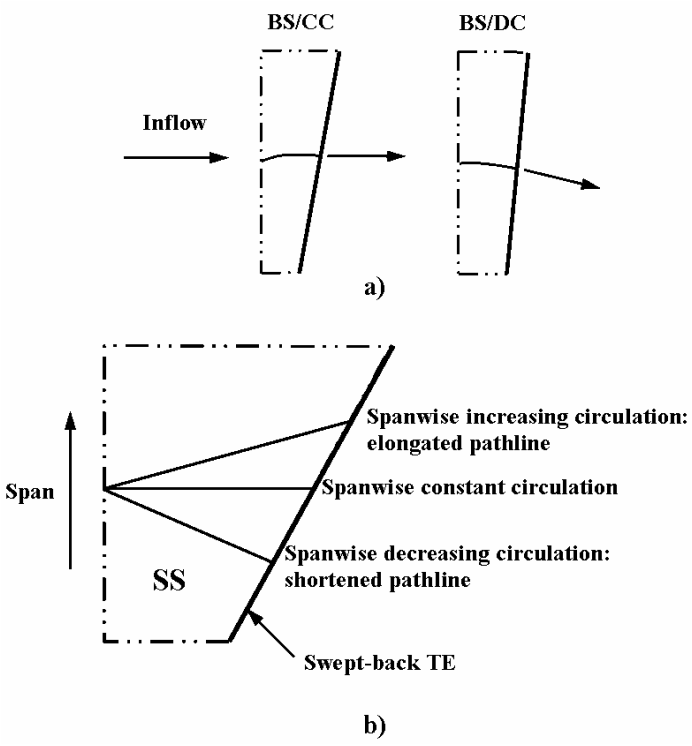

Figure 10. **a)** Computed suction side pathlines near the trailing edges, **b)** Sketch of suction side pathlines for different spanwise circulation gradients

The above suggests that tuning TE sweep and spanwise circulation gradient together can be an aspect for reducing profile losses via reduction of pathline length on the SS near the TE. In the case of swept-forward/swept-back TEs, trailing vorticity according to spanwise increasing/decreasing circulation of appropriate gradient contributes to such pathline reduction, whereas an unswept TE requires spanwise

constant circulation from this aspect. Flow field details reported in [3], [8], [15], and [30] appear to support this pre-concept, already mentioned in the Introduction.

Sweep is often applied in axial flow turbomachines e.g. for noise reduction and improved near-stall behavior. On the other hand, spanwise circulation gradient appears deliberately in blade rows of controlled vortex design. Therefore, both sweep and spanwise circulation gradient are present in certain bladings. Their appropriate tuning may give a potential for efficiency improvement.

6. **Summary**

The results of the case study presented herein are summarized as follows:

1. The studies suggested that regardless of the sweep of the stacking line in itself, the sweep of LE and/or TE causes local unloading of the airfoil. This may enable aerodynamically favorable tuning of chordwise distribution of load.
2. With introduction of equivalent sweep, a model has been proposed to calculate the reduced lift compared to a 2D infinite airfoil in the case of airfoil or blade geometries for which both LE and TE may have sweep, although the stacking line is not necessarily swept. This model represents the results of the present case study better than the classic cos λ law.
3. A possible aspect in reduction of profile losses is reduction of the fluid particle pathline length on the SS. This can be realized via appropriate prescription of forward sweep / no sweep / backward sweep for spanwise increasing / constant / decreasing circulation, respectively, and vice versa.

Acknowledgement. This work has been supported by the Hungarian National Fund for Science and Research under contract No. OTKA T 043493, and by the Széchenyi István Fellowship under contract No. SZÖ 271/2003. Gratitude is expressed to G. Constandinides and T. Régert for the computations, as well as to F. Peretti and M. Gutermuth, who performed the experiments.

REFERENCES

1. Mohammed, K. P. and Prithvi Raj, D.: Investigations on axial flow fan impellers with forward swept blades. *ASME J. Fluids Engineering*, (1977), 543-547.
2. Yamaguchi, N., Tominaga, T., Hattori, S. and Mitsuhashi, T.: Secondary-loss reduction by forward-skewing of axial compressor rotor blading, ASME J. Proc. Yokohama International Gas Turbine Congress, Yokohama, Japan, 1991, II.61-II.68.
3. Wadia, A. R., Szucs, P. N. and Crall, D. W.: Inner workings of aerodynamic sweep. *ASME J. Turbomachinery*, **120**, (1998), 671-682.
4. Wright, T. and Simmons, W. E.: Blade sweep for low-speed axial fans. *ASME J. Turbomachinery*, **112**, (1991), 151-158.
5. Clemen, C. and Stark, U.: Compressor blades with sweep and dihedral: a parameter study, Proc. 5th European Conference Turbomachinery Fluid Dynamics and Thermodynamics, Prague, Czech Republic, 2003, 151-161.

6. Shang, E., Wang, Z. Q. and Su, J. X.: The experimental investigations on the compressor cascades with leaned and curved blade, ASME paper No. 93-GT-50, 1993.
7. Sasaki, T. and Breugelmans, F.: Comparison of sweep and dihedral effects on compressor cascade performance. *ASME J. Turbomachinery*, **120**, (1998), 454-464.
8. Helming, K.: Numerical analysis of sweep effects in shrouded propfan rotors. *J. Propulsion Power*, **12**, (1996), 139-145.
9. Friedrichs, J., Baumgarten, S., Kosyna, G. and Stark, U.: Effect of stator design on stator boundary layer flow in a highly loaded single-stage axial-flow low-speed compressor. *ASME J. Turbomachinery*, **123**, (2001), 483-489.
10. Gümmer, V., Wenger, U. and Kau, H.-P.: Using sweep and dihedral to control three-dimensional flow in transonic stators of axial compressors. *ASME J. Turbomachinery*, **123**, (2001), 40-48.
11. Beiler, M.G. and Carolus T.H.: Computation and measurement of the flow in axial flow fans with skewed blades, ASME J. Turbomachinery, **121**, (1999), 59-66.
12. United States Patent: High efficiency and low weight axial flow fan, Patent No.: US 6, 368, 061 B1, 2002.
13. Braembussche R. A. and Vad J.: Challenges in optimisation of axial flow turbomachinery blades for 3D flow, including sweep and dihedral effects, Summary of workshop organised at the Conference on Modelling Fluid Flow (CMFF'03), 3 to 6 September 2003, Budapest, Hungary. Accepted for publication in Modeling Fluid Flow - State of the Art, Springer Verlag Heidelberg (published in 2004).
14. Glas, W. and Jaberg, H.: Multi-objective evolutionary algorithm for the optimization of swept pump impellers, Proc. 4th European Conference Turbomachinery Fluid Dynamics Thermodynamics, Florence, Italy, 2001, 469-479.
15. Kuhn, K.: Experimentelle Untersuchung einer Axialpumpe und Rohrturbine mit gepfeilten Schaufeln, Dissertation Technische Universität Graz, Institut for Hydraulische Strömungsmaschinen, 2000.
16. Forstner, M., Kuhn, K., Glas, W. and Jaberg, H.: The flow field of pump impellers with forward and backward sweep, Proc. 4th European Conference Turbomachinery Fluid Dynamics Thermodynamics, Florence, Italy, 2001, 577-587.
17. Vad, J. and Corsini, A.: Comparative investigation on axial flow industrial fans of high specific performance with unswept and forward swept blades at design and off-design conditions, Proc. 9th International Symposium Transport Phenomena Dynamics Rotating Machinery, Honolulu, Hawaii, USA. Log. No. FD-ABS-016. CD-ROM, 2002.
18. Vad J., Kwedikha A. R. A. and Jaberg H.: Influence of blade sweep on the energetic behaviour of axial flow turbomachinery rotors at design flow rate, Accepted for 2004 ASME TURBO EXPO. ASME Paper GT2004-53544., 2004.
19. Smith, L. M. and Yeh, H.: Sweep and dihedral effects in axial-flow turbomachinery. *ASME J. Basic Engineering*, **85**, (1963), 401-416.
20. Vad, J., Constandinides, G., Peretti, F., Gutermuth, M. and Régert, T.: Investigation on combined effects of sweep and spanwise changing design circulation on airfoil aerodynamics, Proc. Conference on Modelling Fluid Flow, CMFF'03, Budapest, Hungary, 2003, 145-152.
21. Wallis, R. A.: Wind tunnel tests on a series of circular arc plate airfoils, A.R.L. Aero Note 74., 1946.

22. Corsini, A., Rispoli, F. and Vad, J.: Iterative development of axial flow fans of high specific performance with swept blades, Proc. 5th European Conference Turbomachinery Fluid Dynamics and Thermodynamics, Prague, Czech Republic, 2003, 245-256.

23. FLUENT 6 User's Guide. Fluent Inc., Lebanon, NH, USA, 2001.

24. Borello, D., Corsini, A. and Rispoli, F.: A finite element overlapping scheme for turbomachinery flows on parallel platforms. *Computers & Fluids*, **32**, (2003), 1017-1047.

25. Spalart, P. and Allmaras, S.: *A One-Equation Turbulence Model for Aerodynamic Flows*. AIAA Technical Report AIAA-92-0439, 1992.

26. Gallimore, S. J., Bolger, J. J., Cumpsty, N. A., Taylor, M. J., Wright, P. I. and Place, J. M. M.: The use of sweep and dihedral in multistage axial flow compressor blading - Parts I and II. *ASME J. Turbomachinery*, **124**, (2002), 521-541.

27. Denton, J. D. and Xu, L.: The exploitation of 3D flow in turbomachinery design, In Turbomachinery Design Systems, Von Karman Institute for Fluid Dynamics, Belgium, Lecture Series 1999-02, 1999.

28. Beiler, M. G.: Untersuchung der dreidimensionalen Strömung durch Axialventilatoren mit gekrümmten Schaufeln, Dissertation Universität Siegen. VDI-Verlag, Reihe 7, No. 298, Düsseldorf, 1996.

29. Vad, J. and Bencze, F.: Three-dimensional flow in axial flow fans of non-free vortex design. *Int. J. Heat Fluid Flow*, **19**, (1998), 601-607.

30. Corsini, A., Rispoli, F., Vad, J. and Bencze, F.: Effects of Blade Sweep in a High Performance Axial Flow Rotor, ATI-CST paper 005/01, Proc. 5th European Conference Turbomachinery Fluid Dynamics and Thermodynamics, Italy, 2001, 63-76.